Energy Harvesting Study of Piezoelectric Vibration Harvester with Double Parallel Slender Structure

Xiang Zhao[(✉)] and Haotian Jiang

School of Civil Engineering and Surveying, Southwest Petroleum University, Chengdu 610500, People's Republic of China
`zhaoxiang_swpu@126.com`

Abstract. In this paper, we use a cantilevered double parallel slender structure single deformation piezoelectric energy harvester as a model and combine it with the Lamb-Oseen vortex model, where the effect from fluid vortices is used as an external load, and a metal sheet is attached to the free end of the energy harvester for capturing the shear force generated by wind-generated vortices on the double beams model. The closed-form solution of the bending forced vibration of the piezoelectric energy harvester is solved by establishing the relevant model and deriving the equations. Euler- Bernoulli beam assumptions are used to develop a coupled electromechanical model for the harvester with an intermediate spring layer and a transverse damping is considered, and Green's functions and Laplace transform techniques are used to solve the vibration equations for the coupled piezoelectric vibration system. By solving for the voltage as a function of Green's functions and using Matlab software, we can obtain the functional relationship between the voltage of the harvester and the elastic coefficient of the interlayer and the position of the metal plate setting.

Keywords: Piezoelectric energy harvester · Euler- Bernoulli beam model · Green's function · Laplace transform · Vortex-induced vibration

1 Modeling of Piezoelectric Energy Harvester with Cantilevered Double Straight Beams

1.1 Mechanical Equilibrium Control Equations with Electrically Coupled Effects

This paper investigates a cantilevered double-beam single-deformation piezoelectric energy harvester, which is subjected to external irregularly distributed loads P_1, P_2. As shown in Fig. 1, the energy harvester is based on a homogeneous Eulerian beam model, which consists of a combination of an upper piezoelectric layer and a lower structural layer of the beam system, and the length of the piezoelectric beams are assumed to be L.
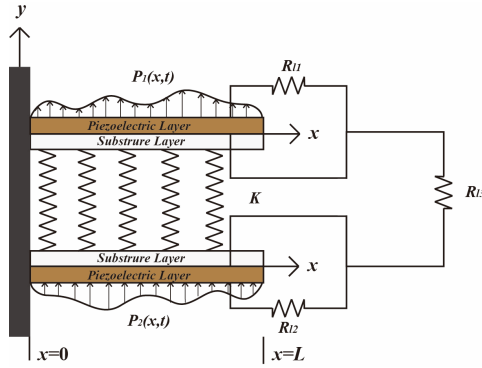
Fig. 1. Cantilevered double beams single deformation piezoelectric energy harvester
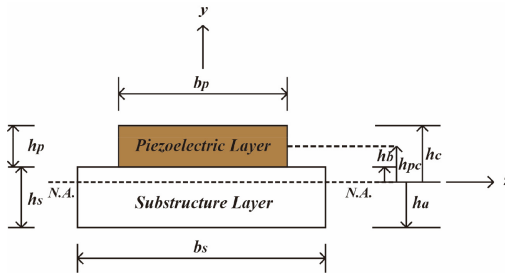

Fig. 2. Cross-section of piezoelectric energy harvester

Figure 2 shows a cross-section of a single-deformation piezoelectric energy harvester, where: b_s is the width of the beam structural layer; b_p is the width of the piezoelectric layer; h_s is the width of the beam structural layer; h_p is the thickness of the piezoelectric layer; h_a is the distance from the neutral axis (NA) to the lowermost surface of the beam structural layer; h_b is the distance from the neutral axis (NA) to the bottom of the piezoelectric layer, and h_c is the distance from the neutral axis (NA) to the top surface of the piezoelectric layer.

When we consider an air damping coefficient c_a, the vibration control equations for a double beams system can be written as [1–3]:

$$\frac{\partial^2 M_1(x, t)}{x^2} + c_a \frac{\partial w_{rel1}(x, t)}{\partial t} + m \frac{\partial^2 w_{rel1}(x, t)}{\partial t^2} + K(w_1 - w_2) = P_1 \qquad (1)$$

$$\frac{\partial^2 M_2(x, t)}{x^2} + c_a \frac{\partial w_{rel2}(x, t)}{\partial t} + m \frac{\partial^2 w_{rel2}(x, t)}{\partial t^2} + K(w_2 - w_1) = P_2 \qquad (2)$$

where $\partial w_{rel}(x, t)$ is the transverse deflection of the beam, $M(x, t)$ is the internal bending moment of the beam, c_a is the viscous air damping coefficient, and m is the mass per unit length of the beam.

In order to obtain an expression for the internal bending moment $M(x, t)$ of the beams, we can utilize the intrinsic relationship between the piezoelectric layer and the structural layer of the beams [4], and brought into the Eqs. (1)(2):

$$
(EI)_{eff} \frac{\partial^4 w_{rel1}(x, t)}{\partial x^4} + c_a \frac{\partial w_{rel1}(x, t)}{\partial t} + m \frac{\partial^2 w_{rel1}(x, t)}{\partial t^2} + K(w_1 - w_2)
$$
$$
+ \vartheta v_1(t) \left[\frac{d\delta(x - x_1)}{dx} - \frac{d\delta(x - x_2)}{dx} \right] = P_1 \tag{3}
$$

$$
(EI)_{eff} \frac{\partial^4 w_{rel2}(x, t)}{\partial x^4} + c_a \frac{\partial w_{rel2}(x, t)}{\partial t} + m \frac{\partial^2 w_{rel2}(x, t)}{\partial t^2} + K(w_2 - w_1)
$$
$$
+ \vartheta v_2(t) \left[\frac{d\delta(x - x_1)}{dx} - \frac{d\delta(x - x_2)}{dx} \right] = P_2 \tag{4}
$$

where: $\delta(x)$ is the Dirac function, $(EI)_{eff}$ is the bending stiffness of the composite cross-section, ϑ is the coupling coefficient, they can be expressed as:

$$
(EI)_{eff} = \frac{E_s b_s (h_b^3 - h_a^3) + E_p b_p (h_c^3 - h_b^3)}{3} \tag{5}
$$

$$
\vartheta = -\frac{E_p b_p d_{31}}{2h_p} (h_c^2 - h_b^2) \tag{6}
$$

1.2 Control Equations for Circuits with Mechanical Coupling Effects

Equations (3)(4) are the vibration control equations for the double beams system under electrical coupling, we utilize the following piezoelectric intrinsic relations [4]:

$$
D_y(x, t) = d_{31} E_p \varepsilon_{xx}(x, t) - \varepsilon_{33}^s \frac{v(t)}{h_p} \tag{7}
$$

where $D_y(x, t)$ is the potential shift parallel to the beam thickness direction, ε_{33}^s is the dielectric constant, and $\varepsilon_{xx}(x, t)$ is the average bending strain.

The bending deformation of the structure will generate a potential shift in the piezo-electric layer, which will be collected by the electrodes, and the charge can be obtained by integrating the potential shift over the electrode region $q(t)$. Since the current $i_i(t)$ is related to the capacitance, the voltage across the resistor can be expressed as [4]:

$$
v_i(t) = R_{li} i_i(t) = -R_{li} \left[\int_{x_1}^{x_2} d_{31} E_p h_{pc} b_p \frac{\partial^2 w_{reli}(x, t)}{\partial x^2 \partial t} dx - \frac{\varepsilon_{33}^s b_p (x_2 - x_1)}{h_p} \frac{dv_i(t)}{dt} \right] \tag{8}
$$

2 Green's Function Solutions for Piezoelectric Vibrations of Double Straight Beams

2.1 Vibration and Piezoelectric Equations Solving

Assuming that the external transverse loads are time-harmonic loads, we can let the deflections and voltages take a similar form to the following, separating the time parameters from the displacements:

$$p_i(x, t) = P_i(x)e^{i\Omega t}, w(x, t) = W(x)e^{i\Omega t}, v(t) = Ve^{i\Omega t} \tag{9}$$

Substitution of Eq. (9) into Eqs. (3) (4) and (8):

$$W_1'''' + a_2 W_1 + a_4 W_2 = b_2 P_1(x) - b_3 V_1[\delta'(x - x_1) - \delta'(x - x_2)] \tag{10}$$

$$W_2'''' + c_2 W_2 + c_4 W_1 = d_2 P_2(x) - d_3 V_2[\delta'(x - x_1) - \delta'(x - x_2)] \tag{11}$$

$$\frac{i\Omega C_p R_l + 1}{R_l} V_i = -i\Omega\beta \int_{x_1}^{x_2} W_i''(x)dx \tag{12}$$

where:

$$
\begin{aligned}
a_2 &= \frac{i\Omega c_a - \mu_1\Omega^2 + K}{E_1 I_1}, a_4 = -\frac{K}{E_1 I_1}, b_2 = \frac{1}{E_1 I_1}, b_3 = \frac{\vartheta}{E_1 I_1} \\
c_2 &= \frac{i\Omega c_a - \mu_2\Omega^2 + K}{E_2 I_2}, c_4 = -\frac{K}{E_2 I_2}, d_2 = \frac{1}{E_2 I_2}, d_3 = \frac{\vartheta}{E_2 I_2}
\end{aligned}
\tag{13}
$$

For a linear system, the principle of superposition should be satisfied. Therefore, the dynamic response of a double-beam system subjected to loads $P_1(x)$ and $P_2(x)$ is the sum of the responses of the systems subjected to $P_1(x)$ and $P_2(x)$ respectively. This shows that the solution of Eqs. (10) and (11) is the sum of the solutions of the following four cases.

Case 1:

$$W_1'''' + a_2 W_1 + a_4 W_2 = b_2 \delta(x - x_0) \tag{14}$$

$$W_2'''' + c_2 W_2 + c_4 W_1 = 0 \tag{15}$$

where $\delta(\cdot)$ is the Dirac delta function [5, 6] and x_0 denotes the location where the unit harmonic load acts. Laplace transformations of Eqs. (14), (15):

$$
\begin{aligned}
Q(s)\overline{W}_1(s) &= (s^4 + c_2)(s^3 W_1(0) + s^2 W_1'(0) + s W_1''(0) + W_1'''(0) + b_2 e^{-sx_0}) \\
&\quad - a_4(s^3 W_2(0) + s^2 W_2'(0) + s W_2''(0) + W_2'''(0))
\end{aligned}
\tag{16}
$$

$$
\begin{aligned}
Q(s)\overline{W}_2(s) &= (s^4 + a_2)(s^3 W_2(0) + s^2 W_2'(0) + s W_2''(0) + W_2'''(0)) \\
&\quad - c_4(s^3 W_1(0) + s^2 W_1'(0) + s W_1''(0) + W_1'''(0) + b_2 e^{-sx_0})
\end{aligned}
\tag{17}
$$

$$Q(s) = (s^4 + a_2)(s^4 + c_2) - a_4 c_4 \tag{18}$$

Divide $Q(s)$ to the right end of the equations and perform an inverse transformation of $\overline{W}_1(s)$ and $\overline{W}_2(s)$:

$$G_{11}(x, x_0) = H(x - x_0)\phi_{11}(x - x_0) + \phi_{21}(x)W_1(0) + \phi_{31}(x)W_1'(0) + \phi_{41}(x)W_1''(0)$$
$$+\phi_{51}(x)W_1'''(0) + \phi_{61}(x)W_2(0) + \phi_{71}(x)W_2'(0) + \phi_{81}(x)W_2''(0) + \phi_{91}(x)W_2'''(0) \tag{19}$$

$$G_{12}(x, x_0) = H(x - x_0)\phi_{12}(x - x_0) + \phi_{22}(x)W_1(0) + \phi_{32}(x)W_1'(0) + \phi_{42}(x)W_1''(0)$$
$$+\phi_{52}(x)W_1'''(0) + \phi_{62}(x)W_2(0) + \phi_{72}(x)W_2'(0) + \phi_{82}(x)W_2''(0) + \phi_{92}(x)W_2'''(0) \tag{20}$$

The expression of φ are displayed in Appendix A. Using the boundary conditions at $x = 0$, The terms in the Green's functions with a coefficient of 0 can be removed:

$$G_{11}(x, x_0) = H(x - x_0)\phi_{11}(x - x_0) + \phi_{41}(x)W_1''(0)$$
$$+\phi_{51}(x)W_1'''(0) + \phi_{81}(x)W_2''(0) + \phi_{91}(x)W_2'''(0) \tag{21}$$

$$G_{12}(x, x_0) = H(x - x_0)\phi_{12}(x - x_0) + \phi_{42}(x)W_1''(0)$$
$$+\phi_{52}(x)W_1'''(0) + \phi_{82}(x)W_2''(0) + \phi_{92}(x)W_2'''(0) \tag{22}$$

Using the boundary conditions at the end of $x = L$, we can derive the second and third order derivatives of the above equations to obtain the following matrix equation:

$$\begin{bmatrix} \phi_{41}''(L) & \phi_{51}''(L) & \phi_{81}''(L) & \phi_{91}''(L) \\ \phi_{41}'''(L) & \phi_{51}'''(L) & \phi_{81}'''(L) & \phi_{91}'''(L) \\ \phi_{42}''(L) & \phi_{52}''(L) & \phi_{82}''(L) & \phi_{92}''(L) \\ \phi_{42}'''(L) & \phi_{51}'''(L) & \phi_{82}'''(L) & \phi_{92}'''(L) \end{bmatrix} \cdot \begin{bmatrix} W_{1''}(0) \\ W_1'''(0) \\ W_2''(0) \\ W_2'''(0) \end{bmatrix} = \begin{bmatrix} -\phi_{11}''(L - x_0) \\ -\phi_{11}'''(L - x_0) \\ -\phi_{12}''(L - x_0) \\ -\phi_{12}'''(L - x_0) \end{bmatrix} \tag{23}$$

Case 2:

The Green's functions for case 2 can be obtained by solving the following equations:

$$W_1'''' + a_2 W_1 + a_4 W_2 = 0 \tag{24}$$

$$W_2'''' + c_2 W_2 + c_4 W_1 = d_2 \delta(x - x_0) \tag{25}$$

The solution process is similar to case 1, its Green's functions are expressed as:

$$G_{21}(x, x_0) = H(x - x_0)\overline{\phi}_{11}(x - x_0) + \phi_{41}(x)W_1''(0)$$
$$+\phi_{51}(x)W_1'''(0) + \phi_{81}(x)W_2''(0) + \phi_{91}(x)W_2'''(0) \tag{26}$$

$$G_{22}(x, x_0) = H(x - x_0)\overline{\phi}_{12}(x - x_0) + \phi_{42}(x)W_1''(0)$$
$$+\phi_{52}(x)W_1'''(0) + \phi_{82}(x)W_2''(0) + \phi_{92}(x)W_2'''(0) \tag{27}$$

The expression of $\overline{\varphi}$ are displayed in Appendix A. According to the superposition principle, the displacement solution can be expressed as:

$$\begin{bmatrix} W_{11}(x) \\ W_{21}(x) \end{bmatrix} = \int_0^L \begin{bmatrix} G_{11}(x; \xi) \\ G_{12}(x; \xi) \end{bmatrix} P_1(\xi) + \begin{bmatrix} G_{21}(x; \xi) \\ G_{22}(x; \xi) \end{bmatrix} P_2(\xi) d\xi \tag{28}$$

Case 3:

The Green's functions for case 3 can be obtained by solving the following equations:

$$W_1'''' + a_2 W_1 + a_4 W_2 = b_3 V_1 \delta'(x - x_0) \tag{29}$$

$$W_2'''' + c_2 W_2 + c_4 W_1 = 0 \tag{30}$$

The Green's functions can be solved in a similar way:

$$
\begin{aligned}
G_{31}(x, x_0) &= V_1 H(x - x_0)\overline{\overline{\phi}}_{11}(x - x_0) + \phi_{41}(x)W_1''(0) \\
&+ \phi_{51}(x)W_1'''(0) + \phi_{81}(x)W_2''(0) + \phi_{91}(x)W_2'''(0)
\end{aligned} \tag{31}
$$

$$
\begin{aligned}
G_{32}(x, x_0) &= V_1 H(x - x_0)\overline{\overline{\phi}}_{12}(x - x_0) + \phi_{42}(x)W_1''(0) \\
&+ \phi_{52}(x)W_1'''(0) + \phi_{82}(x)W_2''(0) + \phi_{92}(x)W_2'''(0)
\end{aligned} \tag{32}
$$

The expression of $\overline{\overline{\varphi}}$ are displayed in Appendix A.

Case 4:

The Green's functions for case 4 can be obtained by solving the following equations:

$$W_1'''' + a_2 W_1 + a_4 W_2 = 0 \tag{33}$$

$$W_2'''' + c_2 W_2 + c_4 W_1 = d_3 V_2 \delta'(x - x_0) \tag{34}$$

The Green's functions can be solved in a similar way:

$$
\begin{aligned}
G_{41}(x, x_0) &= V_2 H(x - x_0)\hat{\phi}_{11}(x - x_0) + \phi_{41}(x)W_1''(0) \\
&+ \phi_{51}(x)W_1'''(0) + \phi_{81}(x)W_2''(0) + \phi_{91}(x)W_2'''(0)
\end{aligned} \tag{35}
$$

$$
\begin{aligned}
G_{42}(x, x_0) &= V_2 H(x - x_0)\hat{\phi}_{12}(x - x_0) + \phi_{42}(x)W_1''(0) \\
&+ \phi_{52}(x)W_1'''(0) + \phi_{82}(x)W_2''(0) + \phi_{92}(x)W_2'''(0)
\end{aligned} \tag{36}
$$

The expressions of $\hat{\varphi}$ are displayed in Appendix A. According to the superposition principle, the displacements W_{12} and W_{22} can be expressed by the Green's functions G_{31}, G_{32}, G_{41}, G_{42} and can be expressed as the following volume integrals.

$$
\begin{aligned}
\begin{bmatrix} W_{12}(x) \\ W_{22}(x) \end{bmatrix} &= \int_0^L \begin{bmatrix} G_{31}(x; \xi) \\ G_{32}(x; \xi) \end{bmatrix} [\delta(\xi - x_2) - \delta(\xi - x_1)] \\
&+ \begin{bmatrix} G_{41}(x; \xi) \\ G_{42}(x; \xi) \end{bmatrix} [\delta(\xi - x_2) - \delta(\xi - x_1)]d\xi
\end{aligned} \tag{37}
$$

2.2 Decoupling of Electromechanical Eulerian Double Beams Systems

According to the principle of superposition of linear systems, the steady state displacement W_1 can be divided into W_{11}, W_{12} two parts; similarly W_2 can be divided into W_{21}, W_{22} two parts. So, the expressions for W_1 and W_2 are:

$$W_1 = W_{11} + W_{12} = \int_0^L G_{11}(x; \xi)P_1(\xi) + G_{21}(x; \xi)P_2(\xi)d\xi$$

$$+ \int_0^L G_{31}(x; \xi)[\delta(\xi - x_2) - \delta(\xi - x_1)] + G_{41}(x; \xi)[\delta(\xi - x_2) - \delta(\xi - x_1)]d\xi$$

(38)

$$W_2 = W_{21} + W_{22} = \int_0^L G_{12}(x; \xi)P_1(\xi) + G_{22}(x; \xi)P_2(\xi)d\xi$$

$$+ \int_0^L G_{32}(x; \xi)[\delta(\xi - x_2) - \delta(\xi - x_1)] + G_{42}(x; \xi)[\delta(\xi - x_2) - \delta(\xi - x_1)]d\xi$$

(39)

Substituting Eqs. (38) (39) into Eq. (8) yields a functional relationship between the voltage and the Green's functions for the four cases:

$$m_1 V_1 = m_2 + m_3 V_2$$
$$n_1 V_2 = n_2 + n_3 V_1$$

(40)

$$m_1 = \left(\frac{i\Omega C_p R_l + 1}{R_l} \right) + i\Omega\beta \int_{x_1}^{x_2} \overline{G}_{31}''(x; x_2) - \overline{G}_{31}''(x; x_1)dx$$

$$m_2 = -i\Omega\beta \int_{x_1}^{x_2} \left[\int_0^L G_{11}(x; \xi)P_1(\xi) + G_{21}(x; \xi)P_2(\xi)d\xi \right]'' dx$$

$$m_3 = -i\Omega\beta \int_{x_1}^{x_2} \overline{G}_{41}''(x; x_2) - \overline{G}_{41}''(x; x_1)dx$$

(41)

$$n_1 = \left(\frac{i\Omega C_p R_l + 1}{R_l} \right) + i\Omega\beta \int_{x_1}^{x_2} \overline{G}_{42}''(x; x_2) - \overline{G}_{42}''(x; x_1)dx$$

$$n_2 = -i\Omega\beta \int_{x_1}^{x_2} \left[\int_0^L G_{12}(x; \xi)P_1(\xi) + G_{22}(x; \xi)P_2(\xi)d\xi \right]'' dx$$

$$n_3 = -i\Omega\beta \int_{x_1}^{x_2} \overline{G}_{32}''(x; x_2) - \overline{G}_{32}''(x; x_1)dx$$

The expressions for voltage we can easily derive from the algebraic Eq. (40) through the linear expressions for voltage V_1 and voltage V_2:

$$V_1 = \frac{m_2 n_1 + m_3 n_2}{m_1 n_1 - m_3 n_3}, \quad V_2 = \frac{m_1 n_2 + m_2 n_3}{m_1 n_1 - m_3 n_3}$$

(42)

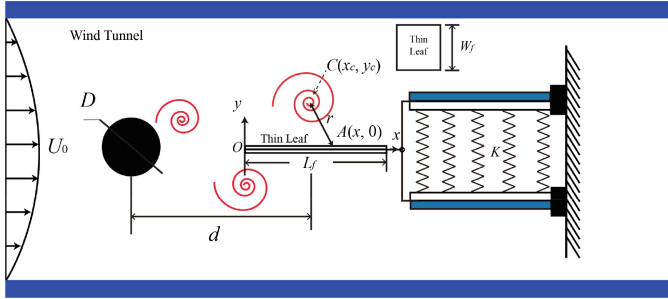# 3   Eddy-Current Induced Vibration of Piezoelectric Energy Harvester

Fig. 3. Schematic diagram of a piezoelectric energy harvester subjected to vortex shedding aerodynamic loads

As shown in Fig. 3, vortex shedding will generate aerodynamic loads. The Lamb-Oseen vortex model [7], which is used in this system, produces a vertical load that can be expressed as [8]:

$$F_v = -\frac{1}{2} W_f \rho_a \int_0^{L_f} (v_c \Phi r - \frac{\Phi^2 r^2}{4}) dx \tag{43}$$

where ρ_a is the air density; W_f and L_f are the width and length of the sheet, respectively; D is the diameter of the solid cylinder, which is an immovable obstacle; U_0 is the mean fluid velocity; $r = ((x - x_c)^2 + y_c^2)^{0.5}$ is the distance from the point $A(x, 0)$ on the sheet to the center $C(x_c, y_c)$ of the vortex, where (x_c, y_c) is the position and v_c is the velocity of the center of the vortex; and the vortex strength Φ is:

$$\Phi = (\Gamma_0 / 4\pi v_e t) exp(-r_0^2 / 4 v_e t) \tag{44}$$

where $\Gamma_0 = (U_0 D)/2S_t$ is the initial velocity cycle, S_t is the Strouhal number related to the Reynolds number, r_0 is the radius of the rigid vortex core [8], v_e is the equivalent dissipation factor of the vortex, $t = d_r/U_0$, d_r is the relative distance between the vortex center and the plate. In this study, the Reynolds number of $S_t = 0.21$ ranges from 10^3 to 10^5, corresponds to a flow rate of 0.05 to 5 m/s. In addition, U_0 can be expressed by the velocity v_c [8].

When the vortex center is located at $y_c = 1.3 \times D/2$, the vortex coming off the cylinder is stable. When the vortex moves to the middle of the thin lobe, the equivalent harmonic force F_v reaches its maximum value, i.e. $x_c = L_f/2$, $d_r = d$. Therefore, the expression of $F_{\max}$ [8]:

$$F_{\max} = -\frac{1}{2} W_f \rho_a \int_0^{L_f} \{\Phi v_c \sqrt{(x - \frac{L_f}{2})^2 + (\frac{1.3D}{2})^2} - \frac{\Phi^2}{4}[(x - \frac{L_f}{2})^2 + (\frac{1.3D}{2})^2]\} dx \tag{45}$$

Substituting into Eq. (42) gives the expression for the voltage:

$$V_1 = -\frac{i\Omega\beta \int_{x_1}^{x_2} \left[G_{11}''(x; L)\lambda F_{max} + G_{21}''(x; L)(1 - \lambda)F_{max} \right]dx \times n_1}{m_1 n_1 - m_3 n_3}$$

$$-\frac{m_3 \times i\Omega\beta \int_{x_1}^{x_2} \left[G_{12}''(x; L)\lambda F_{max} + G_{22}''(x; L)(1 - \lambda)F_{max} \right]dx}{m_1 n_1 - m_3 n_3} \quad (46)$$

$$V_2 = -\frac{m_1 \times i\Omega\beta \int_{x_1}^{x_2} \left[G_{12}''(x; L)\lambda F_{max} + G_{22}''(x; L)(1 - \lambda)F_{max} \right]dx}{m_1 n_1 - m_3 n_3}$$

$$-\frac{i\Omega\beta \int_{x_1}^{x_2} \left[G_{11}''(x; L)\lambda F_{max} + G_{21}''(x; L)(1 - \lambda)F_{max} \right]dx \times n_3}{m_1 n_1 - m_3 n_3} \quad (47)$$

$$V = V_1 + V_2 \quad (48)$$

4 Numerical Analysis

Through the computational derivation of the theory, we can get the expression of the voltage generated by the base model under vortex-induced vibration. In the following, we will explore the effects of different external excitation distributions and elasticity coefficients of springs on the voltage by setting up two sub-models without changing the boundary conditions and Green's functions, respectively.

4.1 Effect of External Excitation Distribution on Voltage

Since the position of the metal sheet in this model can be moved up and down, thus the magnitude of the external excitation force received by the two beams in the vibration model of the cantilevered double beams system can be changed, as shown in Fig. 4. We modeled the data by Matlab software, and after numerical analysis, we can get the magnitude of the voltage collected by the piezoelectric trap in different cases. As shown in Figs. 5, 6, 7.

In this model λ is the external excitation distribution coefficient. Therefore the external excitation forces on the two beams are $F_{v1} = \lambda F_v$ and $F_{v2} = (1 - \lambda)F_v$ respectively.

Figures 5 and 6 show us the relationship between the voltage of the piezoelectric energy harvester and the frequency of the external excitation force, respectively. Since the physical properties of the two beams are set up the same way, the two beams produce peak voltages at the same frequency of the external excitation force, which is 3388 Hz as well as 9317 Hz. When we change the Lambda (i.e., we change the magnitude of the external excitation force applied to the two beams), the performance of the piezoelectric energy
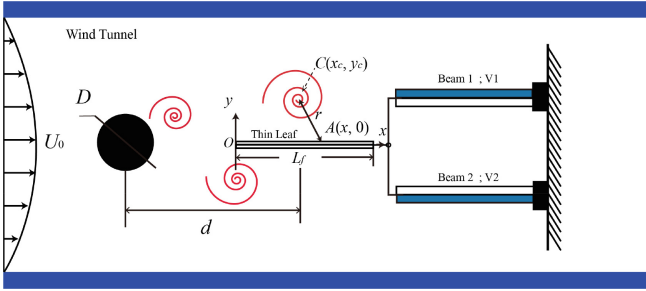
Fig. 4. Schematic diagram of piezoelectric energy harvester subjected to vortex shedding aerodynamic loads (without considering the spring layer)
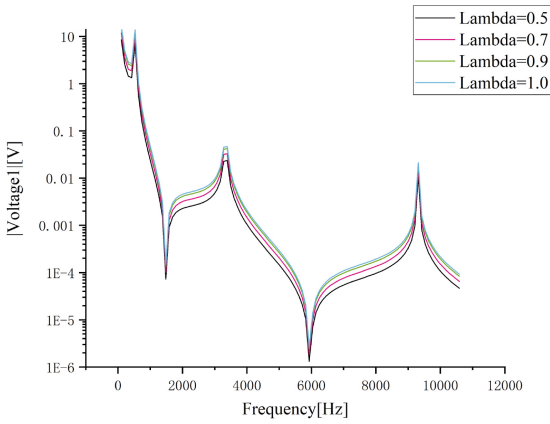

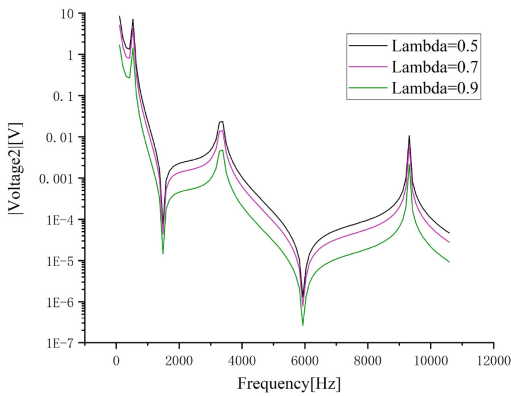**Fig. 5.** Variation of V1 with aerodynamic load excitation frequency for different lambda

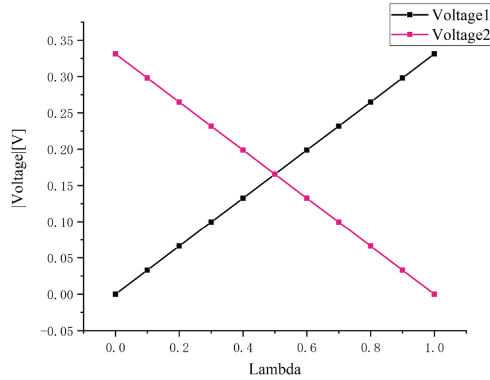**Fig. 6.** Variation of V2 with aerodynamic load excitation frequency for different lambda

Fig. 7. Variation of piezoelectric energy harvester Voltage with Lambda when $\Omega = 2661$

harvester's power generation changed, but it did not affect the frequency magnitude of the external excitation force corresponding to the peak voltage.

From Fig. 7, it can be seen that the voltage of the piezoelectric energy harvester varies linearly with the magnitude of the external excitation force for a certain frequency of the external excitation force, and the sum of the voltages generated by the two beams is a constant value.

4.2 Influence of the Elasticity Coefficient of the Middle Layer on the Voltage of a Piezoelectric Energy Harvester

In this model, as shown in Fig. 8. The two piezoelectric energy harvesters have a spring layer with an elasticity coefficient of K between them. An external excitation force of magnitude both $0.5F_v$ is transmitted to the piezoelectric energy harvesters by setting two identical metal sheets mounted on the cantilever end of each of the two beams. Thus, the relationship between the elasticity coefficient of the middle layer and the voltage of the piezoelectric energy harvester is explored, as shown in Fig. 9.
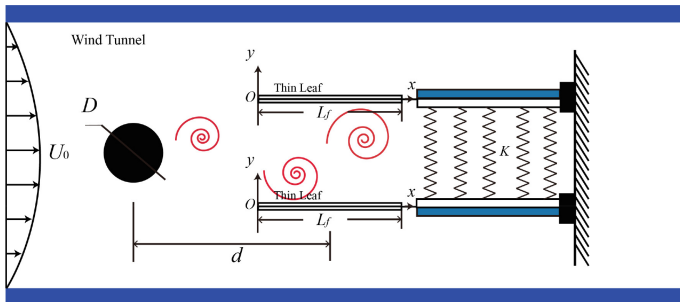

Fig. 8. Schematic of a piezoelectric energy harvester with an intermediate layer subject to vortex shedding aerodynamic loading
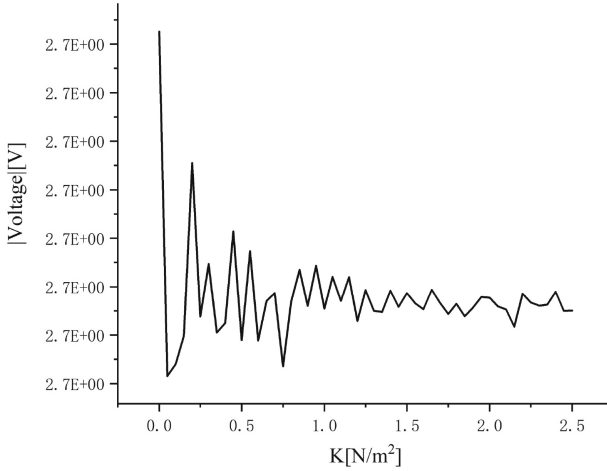
Fig. 9. Variation of piezoelectric energy harvester voltage with elasticity coefficient of the middle layer, $\Omega = 2661$.

Figure 9 shows the change rule of piezoelectric energy harvester voltage with the elasticity coefficient of the intermediate layer K when $\Omega = 2661$. From this figure, it can be seen that: the power generation is highest when the intermediate layer is not added; when the elasticity coefficient is in the range of 0–0.7, the power generation efficiency of the double-beam system is fluctuating; when the elasticity coefficient is greater than 0.7, the constraint capacity of the double-beam system is strong, and the voltage fluctuates in a small range but the overall are smaller than the voltage of not adding the spring layer The voltage of the double-cantilever beams system fluctuates in a small range, but is generally smaller than that without the spring layer. Thus, the addition of an intermediate spring layer to the energy harvester of the double cantilever beams has an inhibiting effect on the power generation efficiency, and when the elasticity coefficient is too large, the generated voltage will gradually converge to a constant value.

5   Conclusions

In this paper, we build a double parallel cantilever energy harvesting system by using the vortex excitation force generated by vortex shedding as the external load. We discuss the effects of different sizes of external loads on the power generation efficiency of the dual-beam system; we also explore the effects on the voltage magnitude with the addition of an intermediate spring layer. The following are the main conclusions of this paper.

(1) The voltage of each beam of the energy harvester of the double-parallel structure varies linearly with the magnitude of the external excitation force, but does not affect the frequency of the external excitation force corresponding to the peak voltage.
(2) The addition of an intermediate layer will reduce the power generation efficiency of the double-parallel cantilever energy harvester to a certain extent, and the voltage will be bullied to fluctuate; when the elasticity coefficient of the intermediate layer is large, the voltage is suppressed and tends to be constant.

Appendix A

$$\overline{\phi}_{11}^{(k)}(x) = -\sum_{i=1}^{8} s_i^k A_i(x) a_4 d_2; \; \overline{\phi}_{12}^{(k)}(x) = \sum_{i=1}^{8} s_i^k A_i(x)(s_i^4 + a_2)d_2$$

$$\overline{\overline{\phi}}_{11}(x) = \sum_{i=1}^{8} A_i(x)(s_i^4 + c_2)b_3 s_i; \; \overline{\overline{\phi}}_{12}(x) = -\sum_{i=1}^{8} A_i(x)c_4 b_3 s_i$$

$$\hat{\phi}_{11}(x) = -\sum_{i=1}^{8} A_i(x) a_4 d_3 s_i; \; \hat{\phi}_{12}(x) = \sum_{i=1}^{8} A_i(x)(s_i^4 + a_2)d_3 s_i$$

$$\phi_{11}(x) = \sum_{i=1}^{8} A_i(x)(s_i^4 + c_2)b_2, \; \phi_{21}(x) = \sum_{i=1}^{8} A_i(x)(s_i^4 + c_2)s_i^3$$

$$\phi_{31}(x) = \sum_{i=1}^{8} A_i(x)(s_i^4 + c_2)s_i^2, \; \phi_{41}(x) = \sum_{i=1}^{8} A_i(x)(s_i^4 + c_2)s_i$$

$$\phi_{51}(x) = \sum_{i=1}^{8} A_i(x)(s_i^4 + c_2), \; \phi_{61}(x) = -\sum_{i=1}^{8} A_i(x)a_4 s_i^3$$

$$\phi_{71}(x) = -\sum_{i=1}^{8} A_i(x)a_4 s_i^2, \; \phi_{81}(x) = -\sum_{i=1}^{8} A_i(x)a_4 s_i$$

$$\phi_{91}(x) = -\sum_{i=1}^{8} A_i(x)a_4$$

$$\phi_{12}(x) = -\sum_{i=1}^{8} A_i(x)c_4 b_2, \; \phi_{22}(x) = -\sum_{i=1}^{8} A_i(x)c_4 s_i^3$$

$$\phi_{32}(x) = -\sum_{i=1}^{8} A_i(x)c_4 s_i^2, \; \phi_{42}(x) = -\sum_{i=1}^{8} A_i(x)c_4 s_i$$

$$\phi_{52}(x) = -\sum_{i=1}^{8} A_i(x)c_4, \; \phi_{62}(x) = \sum_{i=1}^{8} A_i(x)(s_i^4 + a_2)s_i^3$$

$$\phi_{72}(x) = \sum_{i=1}^{8} A_i(x)(s_i^4 + a_2)s_i^2, \; \phi_{82}(x) = \sum_{i=1}^{8} A_i(x)(s_i^4 + a_2)s_i$$

$$\phi_{92}(x) = \sum_{i=1}^{8} A_i(x)(s_i^4 + a_2)$$

$$A_i(x) = \frac{e^{s_i x}}{(s_i - s_1)..(s_i - s_{i-1})(s_i - s_{i+1})..(s_i - s_8)} \; (i = 1 \sim 8)$$

References

1. Stojanović, V., Kozić, P., Pavlović, R., et al.: Effect of rotary inertia and shear on vibration and buckling of a double beam system under compressive axial loading. Arch. Appl. Mech. **81**(12), 1993–2005 (2011)
2. Xiaobin, L.I., Shuangxi, X.U., Weiguo, W.U., et al.: An exact dynamic stiffness matrix for axially loaded double-beam systems. Sadhana **39**(3), 607–623 (2014)
3. Zhao, X., Chen, B., Li, Y.H., et al.: Forced vibration analysis of Timoshenko double-beam system under compressive axial load by means of Green's functions. J. Sound Vib. **464**, 115001 (2020)
4. Erturk, A., Inman, D.J.: A distributed parameter electromechanical model for cantilevered piezoelectric energy harvesters. J. Vib. Acoust. **130**(4) (2008)
5. Abu-Hilal, M.: Forced vibration of Euler-Bernoulli beams by means of dynamic Green functions. J. Sound Vib. **267**(2), 191–207 (2003)
6. Li, X.Y., Zhao, X., Li, Y.H.: Green's functions of the forced vibration of Timoshenko beams with damping effect. J. Sound Vib. **333**(6), 1781–1795 (2014)
7. Erratum [M]. Wu, J.-Z., Ma, H.-Y., Zhou, M.-D.: Vorticity and Vortex Dynamics, pp. 777–780. Springer, Heidelberg (2006). https://doi.org/10.1007/978-3-540-29028-5_13
8. Hu, Y., Yang, B., Chen, X., et al.: Modeling and experimental study of a piezoelectric energy harvester from vortex shedding-induced vibration. Energy Convers. Manage. **162**, 145–158 (2018)